OXFORD

SOT | Society of Toxicology
www.toxsci.oxfordjournals.org

TOXICOLOGICAL SCIENCES, 158(2), 2017, 444–453

doi: 10.1093/toxsci/kfx106
Advance Access Publication Date: May 19, 2017
Research Article

ROS-Induced Store-Operated Ca^{2+} Entry Coupled to PARP-1 Hyperactivation Is Independent of PARG Activity in Necrotic Cell Death

Frances M. Munoz,[1] Fengjiao Zhang,[2] Argel Islas-Robles,[3] Serrine S. Lau,[4] and Terrence J. Monks[4,5]

Department of Pharmacology and Toxicology, College of Pharmacy, University of Arizona Health Sciences Center, Tucson, Arizona 85721

[1]Present address: Department of Pharmacology and Physiology, Drexel University College of Medicine, Philadelphia, PA 19102.

[2]Present address: Wu Ya College of Innovation, Shenyang Pharmaceutical University, Shenyang, Liaoning 110016, P. R. China.

[3]Present address: Department of Pharmacology and Toxicology, College of Pharmacy, University of Arizona Health Sciences Center, Tucson, AZ 85721.

[4]Present address: Eugene Applebaum College of Pharmacy and Health Sciences, Wayne State University, Detroit, MI 48201.
[5]To whom correspondence should be addressed at Department of Pharmaceutical Sciences, Eugene Applebaum College of Pharmacy and Health Sciences, 259 Mack Avenue – Suite 5148, Detroit, MI 48201. Fax: (313) 577-0457. E-mail: terrence.monks@wayne.edu.

ABSTRACT

2,3,5-*tris*(Glutathion-S-yl)hydroquinone, a potent nephrotoxic and nephrocarcinogenic metabolite of benzene and hydroquinone, generates reactive oxygen species (ROS) causing DNA strand breaks and the subsequent activation of DNA repair enzymes, including poly(ADP-ribose) polymerase (PARP)-1. Under robust oxidative DNA damage, PARP-1 is hyperactivated, resulting in the depletion of NAD^+ and ATP with accompanying elevations in intracellular calcium concentrations (iCa^{2+}), and ultimately necrotic cell death. The role of Ca^{2+} during PARP-dependent necrotic cell death remains unclear. We therefore sought to determine the relationship between Ca^{2+} and PARP-1 during ROS-induced necrotic cell death in human renal proximal tubule epithelial cells (HK-2). Our experiments suggest that store-operated Ca^{2+} channel (SOC) entry contributes to the coupling of PARP-1 activation to increases in iCa^{2+} during ROS-induced cell death. Poly(ADP-ribose)glycohydrolase (PARG), which catalyzes the degradation of PARs to yield free ADP-ribose (ADPR), is known to activate Ca^{2+} channels such as TRPM2. However, siRNA knockdown of PARG did not restore cell viability, indicating that free ADPR is not responsible for SOC activation in HK-2 cells. The data indicate that PARP-1 and iCa^{2+} are coupled through activation of SOC mediated Ca^{2+} entry in an apparently ADPR-independent fashion; alternative PAR-mediated signaling likely contributes to PARP-dependent necrotic cell death, perhaps via PAR-mediated signaling proteins that regulate iCa^{2+} homeostasis.

Key words: 2,3,5-*tris*(glutathione-S-yl)hydroquinone; HK-2 cells; store-operated calcium channel entry; poly(ADP-ribose)polymerase-1; poly(ADP-ribose)glycohydrolase; PARylation.

2,3,5-*tris*(Glutathion-S-yl)hydroquinone (TGHQ), a potent nephrotoxic and nephrocarcinogenic metabolite of benzene and hydroquinone (HQ), generates reactive oxygen species (ROS) causing DNA strand breaks and the subsequent activation of DNA repair enzymes, including poly(ADP-ribose) polymerase (PARP)-1. PARP-1 is an abundant nuclear protein that contributes to the regulation of chromatin structure, gene expression, DNA metabolism, and DNA repair (Krishnakumar and Kraus, 2010). PARP-1 is activated 500-fold above basal levels by ROS induced DNA strand breaks (Virag *et al.*, 2013). Upon activation by DNA strand breaks and utilizing nicotinamide adenine dinucleotide (NAD^+) as a substrate (D'Amours *et al.*, 1999; Luo

and Kraus, 2012), PARP-1 catalyzes the covalent attachment of poly(ADP-ribose) (PAR) polymers onto acceptor proteins, including proteins that participate in DNA repair, transcription factors, PARP-1 itself, and histones. Whilst PARP-1 has a primary function to regulate and repair DNA, excessive DNA strand breaks lead to PARP-1 overactivation, which subsequently results in depletion of both NAD^+ and ATP, and ultimately cell death (Pieper *et al.*, 1999).

Although the precise molecular events that occur downstream of PARP-1 hyperactivation during PARP-1-mediated cell death remain elusive, substantial NAD^+ depletion can result in the loss of mitochondrial membrane potential, and both caspase-dependent and independent cell death (Kim *et al.*, 2005; Zhang *et al.*, 2012). Moreover, traumas such as ischemia-reperfusion, myocardial infarction, and ROS-induced injury are all known to hyperactivate PARP-1 in scenarios where inhibition of PARP-1 prevents cell death and long-term tissue damage (Jagtap and Szabo, 2005; Kim *et al.*, 2005).

Ca^{2+}-dependent modulation of PARP-1 during cellular stress leads to changes in cell metabolism, and attenuation of ROS-induced cell death (Bentle *et al.*, 2006). Similar to the effects of PARP-1 inhibition, chelation of intracellular Ca^{2+} with BAPTA-AM protects against cell stress (Bentle *et al.*, 2006; Zhang *et al.*, 2014). In particular, Ca^{2+} chelation also attenuates PARP-1 hyperactivation and γ-H2AX formation during ROS-induced cell death. Moreover, inhibition of PARP-1 reduced TGHQ-induced changes in iCa^{2+} (Zhang *et al.*, 2014). Thus, iCa^{2+} appears to be coupled to PARP-1 hyperactivation during ROS-induced cell death. However, mechanisms by which PARP-1 and Ca^{2+} are coupled in a manner that exacerbates cellular stress remain unclear. PARylation, the manner in which PAR polymers bind to proteins, regulates several cellular processes, including DNA repair, chromatin architecture, cell cycle progression, transcription, mitochondrial function, and cell death (Virag *et al.*, 2013). Covalently PARylated proteins can be hydrolyzed to free poly(ADP-ribose) (PAR), or mono(adenosine diphosphate ribose) (ADPR), by poly(ADP-ribose)glycohydrolase (PARG) (Luo and Kraus, 2012). Because of the rapid breakdown of PAR, it can act as a signal transducer, either as a PARG-derived ADPR monomer, or as a free polymer via binding to proteins containing PAR-binding motifs, PAR-binding zinc finger domains, and macrodomains (Gagne *et al.*, 2001; Kraus, 2008). PAR signaling has been implicated in many different forms of cell death, including parthanatos (Andrabi *et al.*, 2006), autophagy (Munoz-Gamez *et al.*, 2009; Rodriguez-Vargas *et al.*, 2012), and regulated necrosis or necroptosis (Virag *et al.*, 1998).

TGHQ, a potent ROS-generating nephrotoxic metabolite of HQ (Lau *et al.*, 2001), causes non-apoptotic cell death in human renal proximal tubule epithelial (HK-2) cells (Zhang *et al.*, 2014). Moreover, TGHQ-induced cell death in HK-2 cells required hyperactivation of PARP-1 coupled to increases in iCa^{2+}, but is independent of apoptosis-inducing factor (AIF) translocation from the mitochondria to the nucleus (Zhang *et al.*, 2014). The current studies further explored the relationship between PARP-1 and iCa^{2+}, including investigations on the role of PARG in ROS-induced cell death and its relationship to the coupling of PARP-1 signaling and iCa^{2+}. Our data reveal that store-operated calcium channels (SOCs) play a role in ROS-mediated cell death and that Ca^{2+} entry through SOCs is coupled to PARP-1 activity. Intriguingly, in contrast to previous reports linking Ca^{2+} to PARP-1 via the breakdown of PAR, our data reveal cell death is independent of PARG activity, suggesting a novel pathway for the coupling of PARP-1 and Ca^{2+} leading to cell death.

MATERIALS AND METHODS

Chemicals, reagents, and TGHQ purification. TGHQ was synthesized and purified as previously described (Lau *et al.*, 1988). TGHQ is nephrotoxic and carcinogenic and must therefore be handled with protective clothing in a ventilated hood. Adenosine 5′-diphosphate (Hydroxymethyl)pyrrolidinediol (ADP-HPD), a cell impermeable PARG inhibitor, was purchased from EMD Millipore (Billerica, Massachusetts). H_2DCFDA and Fluo-4-AM were obtained from Life Technologies (Carlsbad, California). Antibody for poly(ADP-ribose) was a product of Enzo Life Sciences (Farmingdale, New York). All other reagents and chemicals were purchased from Sigma-Aldrich (St. Louis, Missouri).

Cell culture. Human kidney proximal tubule epithelial cells (HK-2) were obtained from the American Type Culture Collection (Manassas, Virginia). Cells were cultured in keratinocyte serum-free medium (K-SFM, Life Technologies, Carlsbad, California) supplemented with 0.05 mg/ml bovine pituitary extract and 5 ng/ml epidermal growth factor provided by the media supplier. Cell cultures were performed at 37°C in a humidified atmosphere of 5% CO_2. Cells were grown to ~80% confluence prior to treatment.

Cell death viability assays-MTS. To determine the viability of HK-2 cells in the presence and absence of various toxicants and inhibitors, cells were seeded at 8×10^3 cells/well and allowed to grow to ~80% confluence. Cells were washed once with Dulbecco's Modified Eagle's Medium (DMEM), without sodium pyruvate, supplemented with 25-mM HEPES, then treated with TGHQ with or without inhibitors. Cell viability was determined with an assay measuring mitochondrial dehydrogenase activity (Promega, Madison, Wisconsin) according to the manufacturer's instructions, in which [3-(4,5-dimethylthiazol-2-yl)-5-(3-carboxymethoxyphenyl)-2-(4-sulfophenyl)-2H-tetrazolium], inner salt (MTS), a tetrazolium compound, is reduced to a formazan product by dehydrogenase enzymes found in metabolically active cells. After treatment with TGHQ, cells were washed twice with DMEM/HEPES without phenol red, MTS (20 μl) was subsequently added to 100 μl of DMEM/HEPES and incubated for 2 h at 37°C. The absorbance of the formazan was measured directly from 96-well plates at 490 nm using a SpectraMax M3 microplate reader (Molecular Devices, Sunnyvale, California).

Measurement of ROS generation. HK-2 cells were seeded in clear bottom black 96-well plates at 8×10^3 cells/well and grown to ~80% confluence. Cells were washed once with DMEM/HEPES without phenol red, then incubated with 10 μM 2′,7′-dichlorodihydrofluorescein diacetate (H_2DCFA) for 30 min at 37°C. Cells were washed twice with DMEM/HEPES without phenol red, and incubated at 37°C for another 30 min in the presence and absence of various inhibitors. Cells were then treated with TGHQ (400 μM) and immediately placed in a SpectraMax M3 microplate reader (Molecular Devices, California). A kinetic assay was performed at 495 nm excitation and 525 nm emission for 1 h, where cells were imaged every 10 min.

Western blot analysis. HK-2 cells were seeded in 6-well plates at 2.0×10^5 cells/well and grown to ~80% confluence. After treatment with TGHQ, cells were washed twice with cold PBS and lysed with PAR lysis buffer containing 50-mM Tris HCl, pH 7.5, 150-mM NaCl, 0.5% deoxycholate, 0.1% SDS, 1-mM EGTA, 1-mM EDTA, 1% Nonidet P-40, 20% glycerol, a complete protease

inhibitor tablet, and 1-μM Adenosine 5′-diphosphate (Hydroxymethyl)pyrrolidinediol (ADP-HPD). Cells were rotated for 15 min at 4°C then centrifuged to remove cell debris. Protein concentrations were determined with detergent-compatible reagent (Bio-Rad Labs, Hercules, California), then lysate was incubated with 4× sample buffer (Bio-Rad Labs, Hercules, California) containing 5% 2-mercaptoethanol, and heated for 15 min at 65°C on a heating block. Samples were resolved in 7.5% SDS-polyacrylamide gels and transferred to polyvinylidene difluoride membranes (EMD Millipore, Billerica, Massachusetts). Membranes were blocked with 5% nonfat milk in Tris-buffered saline with 0.5% Tween 20 (TBS-T), then incubated with primary antibody overnight at 4°C. Following washes, membranes were incubated with secondary antibody coupled with horseradish peroxidase for 1 h at room temperature. Immunoblots were developed using enhanced chemiluminescence reaction (Pierce, Thermo Scientific, Rockwell, Illinois) and imaged on a ChemiDoc XRS System (BioRad, Hercules, California).

Determination of total NAD content. Cells were seeded on 6-well plates at 2.0×10^5 cells/well for 48 h and grown to ~80% confluence. Cells were pretreated with 2-APB, a non-selective SOC channel inhibitor, and then co-treated with TGHQ (400 μM) at indicated treatment times. Total NAD^+ was extracted using 1.0-M $HClO_4$ and neutralized to pH 7.0 by adding 2-M KOH/0.66-M KH_2PO_4. NAD^+ concentrations were determined by enzymatic cycling assays as previously described (Jacobson and Jacobson, 1997) using a SpectraMax M3 microplate reader (Molecular Devices, California).

Live cell calcium imaging. HK-2 cells were seeded on 35-mm ibiTreat tissue culture dishes (Ibidi, Verona, Wisconsin) at 2.0×10^5 cells/dish and cultured for 48 h to ~80% confluence. Cells were rinsed once with DMEM without phenol red containing 25-mM HEPES, then loaded with 5 μM Fluo-4 AM for 30 min at room temperature. Cells were washed 3 times with Hank's Balanced Salt Solution, and subsequently incubated with DMEM/HEPES without phenol red for an additional 30 min at room temperature in the presence and absence of inhibitors. Cells were treated with TGHQ for 2 h at 37°C and immediately imaged at ×40 magnification on a DeltaVision RT deconvolution microscopy system (GE Healthcare Life Sciences, Pittsburg, Pennsylvania) with an inverted Olympus IX 70 microscope controlled by imaging program DeltaVision softWoRx. Data were analyzed using the NIH provided software ImageJ.

siRNA knockdown of PARG. Cells were seeded in 24-well or 96-well plates and allowed to grow to ~25% confluence prior to transfection. Knockdown of PARG was performed using the transfection reagent DharmaFECT along with ON-TARGETplus siRNA SMART pool purchased from Dharmacon (Lafayette, Colorado). Cells were transfected using 25-nM non-targeting siRNA or PARG siRNA and incubated for 72 h, changing culture media daily. Confirmation of knockdown was determined by Western blot analysis.

Immunofluorescence analysis. HK-2 cells were seeded in 35-mm ibiTreat tissue culture dishes at 2.0×10^5 cells/dish and grown to ~80% confluence. Cells were treated with TGHQ (400 μM) for 30 min then rinsed twice with ice cold PBS. Cells were permeabilized and fixed using a 1:1 mixture of acetone and methanol for 20 min at −20°C. Immediately after fixation, cells were rinsed twice with PBS and blocked using 1% bovine serum albumin in PBS containing 1% Tween 20 (PBS-T) for 2 h at room temperature. Cells were incubated with anti-PAR antibody in 1% BSA overnight at 4°C, then washed 3 times with PBS-T the following day. Cells were finally incubated with donkey anti-mouse IgG Alexa 488 (Life Technologies) antibody in 1% BSA for 2 h at room temperature in the dark, then washed with PBS and incubated with DAPI at room temperature for 30 min. Cells were imaged at ×40 magnification using an oil immersion lens on a DeltaVision RT deconvolution microscopy system (GE Healthcare Life Sciences, Pittsburg, Pennsylvania) with an inverted Olympus IX 70 microscope controlled by imaging program DeltaVision SoftWoRx. Data were analyzed using the NIH provided software ImageJ.

Statistical analyses. Statistical differences between the treated and control groups were determined by Student's unpaired *t* test. Differences between groups were assessed by one-way ANOVA using Graphpad Prism 6 for Mac. $P < .05$ was considered to be statistically significant.

RESULTS

Depletion of Intracellular Calcium Stores Does Not Protect Against ROS-Induced Cell Death

TGHQ-generated ROS-induced cell death can be attenuated when increases in iCa^{2+} are impaired by chelation with BAPTA-AM (Zhang *et al.*, 2014). We therefore sought to determine the source(s) of Ca^{2+} contributing to increases in iCa^{2+} to further elucidate the relationship between Ca^{2+} and ROS-induced necrotic cell death. TGHQ decreased cell viability as evidenced by decreases in mitochondrial dehydrogenase activity (Figure 1). In addition, depletion of ER Ca^{2+} stores was accomplished using a sarcoplasmic-endoplasmic reticulum calcium ATPase (SERCA) pump inhibitor, thapsigargin. Thapsigargin binds to the SERCA pump, depleting ER stores within 5 min of treatment, and prevents reentry of Ca^{2+} to replenish stores through the SERCA pump (Figure 1A). Pre-treatment and co-treatment with various concentrations of thapsigargin in the presence of TGHQ (Figure 1B) did not restore mitochondrial dehydrogenase activity, eliminating ER Ca^{2+} stores as a source of increased cytosolic Ca^{2+} during TGHQ-induced cell death.

SOCs Contribute to Increases in Intracellular Calcium

To assess whether extracellular Ca^{2+} was the source of elevations in cytoplasmic Ca^{2+}, store-operated Ca^{2+} channels (SOCs) were inhibited using a common inhibitor, 2-aminoethoxydiphenyl borate (2-APB) (DeHaven *et al.*, 2008). Pre-treatment and co-treatment of cells with 2-APB in the presence of TGHQ restored mitochondrial dehydrogenase activity in a time- (Figure 2B) and dose-dependent manner (Figure 2A), suggesting that SOCs play a role in TGHQ-induced cell death. Live cell Ca^{2+} imaging of cells pre-treated and co-treated with 2-APB and treated with TGHQ (400 μM) revealed a decrease in iCa^{2+} concentrations over 2 h (Figs. 2C and 2D), further confirming that SOCs contribute to TGHQ initiated increases in iCa^{2+}.

SOC Entry Is Coupled to PARP-1 Activation During TGHQ-Induced Necrotic Cell Death

To elucidate the relationship between SOCs with PARP-1, and their respective role in cell death, we examined the effects of SOC inhibition on PARP-1 activity. PARP-1 activation has been coupled to cell death through the consumption of NAD^+, a

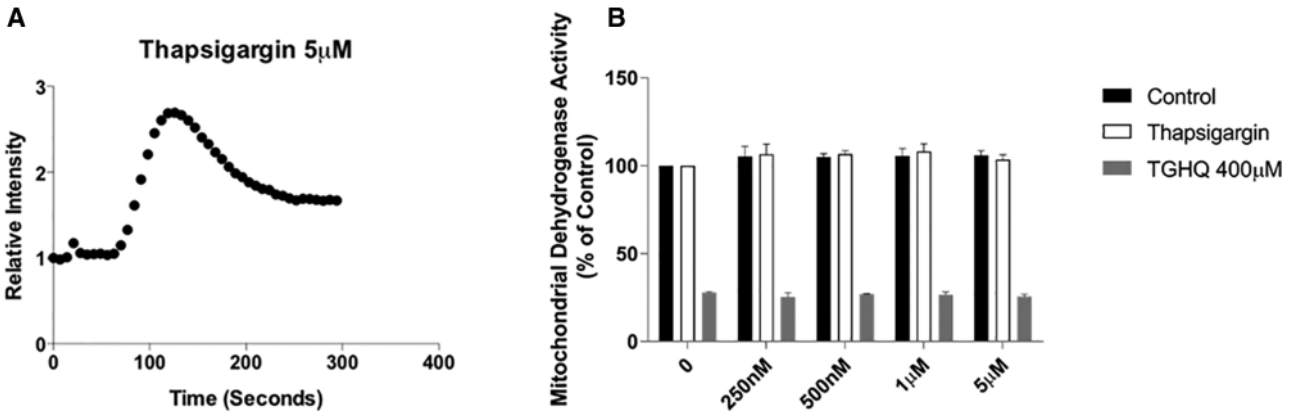

Figure 1. Depletion of intracellular calcium stores by thapsigargin does not protect against TGHQ-induced cell death. (A) Cells were incubated with Fluo-4 AM (5 μM) for 30 min at room temperature, then left another 20 min at room temperature. An area of the cells was recorded every 7 s for 5 min during the addition of thapsigargin (5 μM) to determine levels of iCa^{2+}. Data represent relative intensity to that at time 0 s. (B) HK-2 cells were pre-treated for 30 min and then co-treated with thapsigargin at various concentrations in the presence or absence of TGHQ 400 μM for 2 h. Cell viability was determined using MTS-based assay. Formazan formation relative to untreated cells (% control) represents cell viability after treatment. Data are mean ± SE; $n \geq 3$.

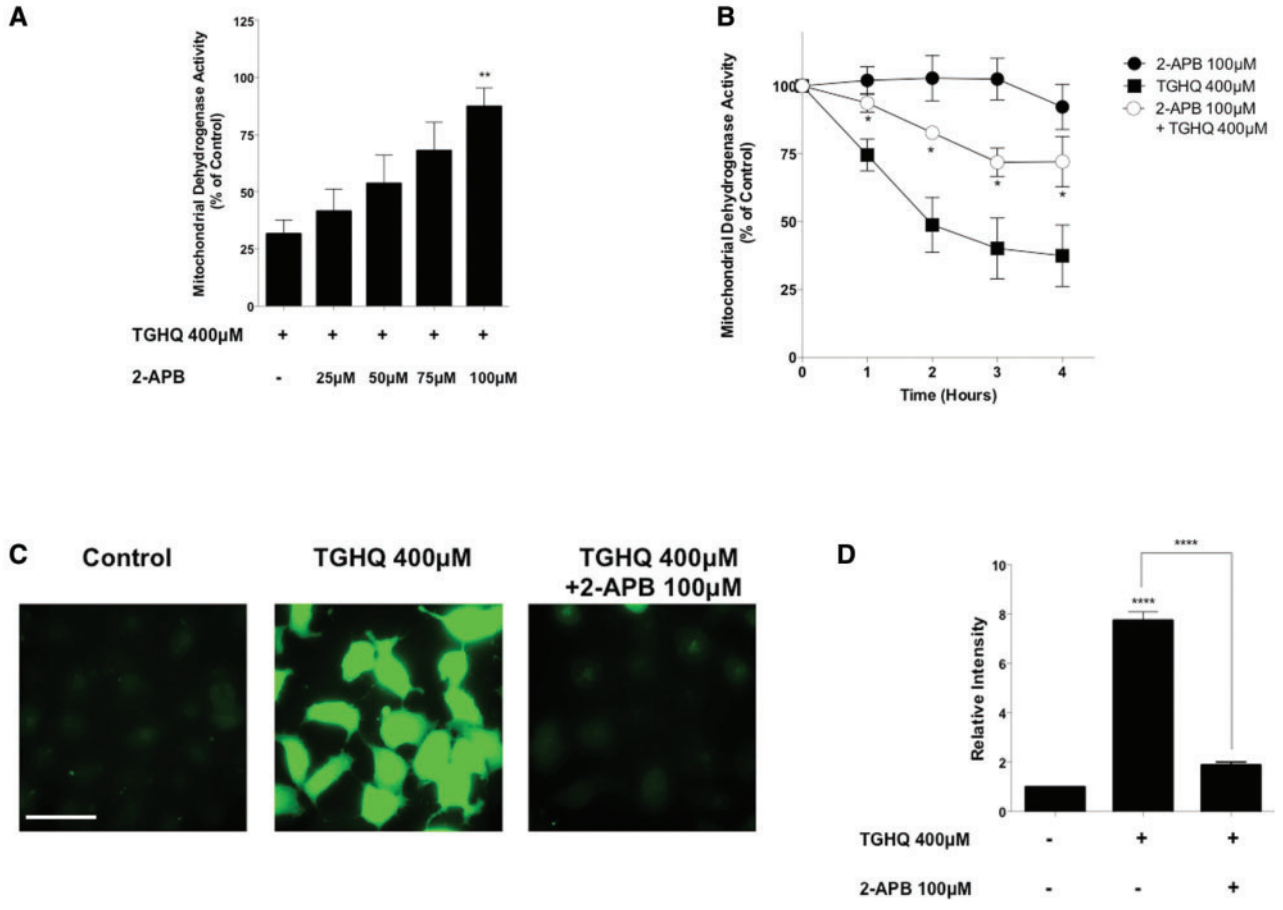

Figure 2. SOCs facilitate increases in intracellular calcium. (A) HK-2 cells were pre-treated for 30 min and co-treated with SOC inhibitor 2-APB at various concentrations (25–100 μM) in the presence or absence of TGHQ 400 μM for 2 h. (B) HK-2 cells were pre-treated for 30 min and co-treated with 2-APB (100 μM) in the presence of TGHQ 400 μM for various periods of time (1–4 h). Cell viability was determined using the MTS based assay. (C) Cells were incubated with Fluo-4 AM (5 μM) and pre-treated with 2-APB (100 μM), then co-treated with TGHQ 400 μM for 2 h. Cells were immediately imaged using ×40 magnification under a deconvolution microscope. Scale bar 100 μm. (D) The densitometric and statistical analysis of the calcium imaging data. All data are mean ± SE; $n \geq 3$. *$P < .05$, **$P < .01$ when compared with TGHQ by one-way ANOVA followed by a post-hoc Tukey's test. ****$P < .001$ when compared with control by one-way ANOVA followed by a post-hoc Tukey's test.

cofactor necessary for the PARylation of proteins. Total NAD^+ levels were depleted by >50% within 2 h of treatment with TGHQ (Figs. 3A and 3B). Moreover, pre-treatment and co-treatment of cells with 2-APB restored NAD^+ levels in both a time- (Figure 3B) and dose-dependent manner (Figure 3A), indicating an interaction between SOCs and PARP-1. Western blot analysis of PAR confirmed that pre-treatment and co-treatment with 2-APB attenuated ribosylation initiated by PARP-1 in the

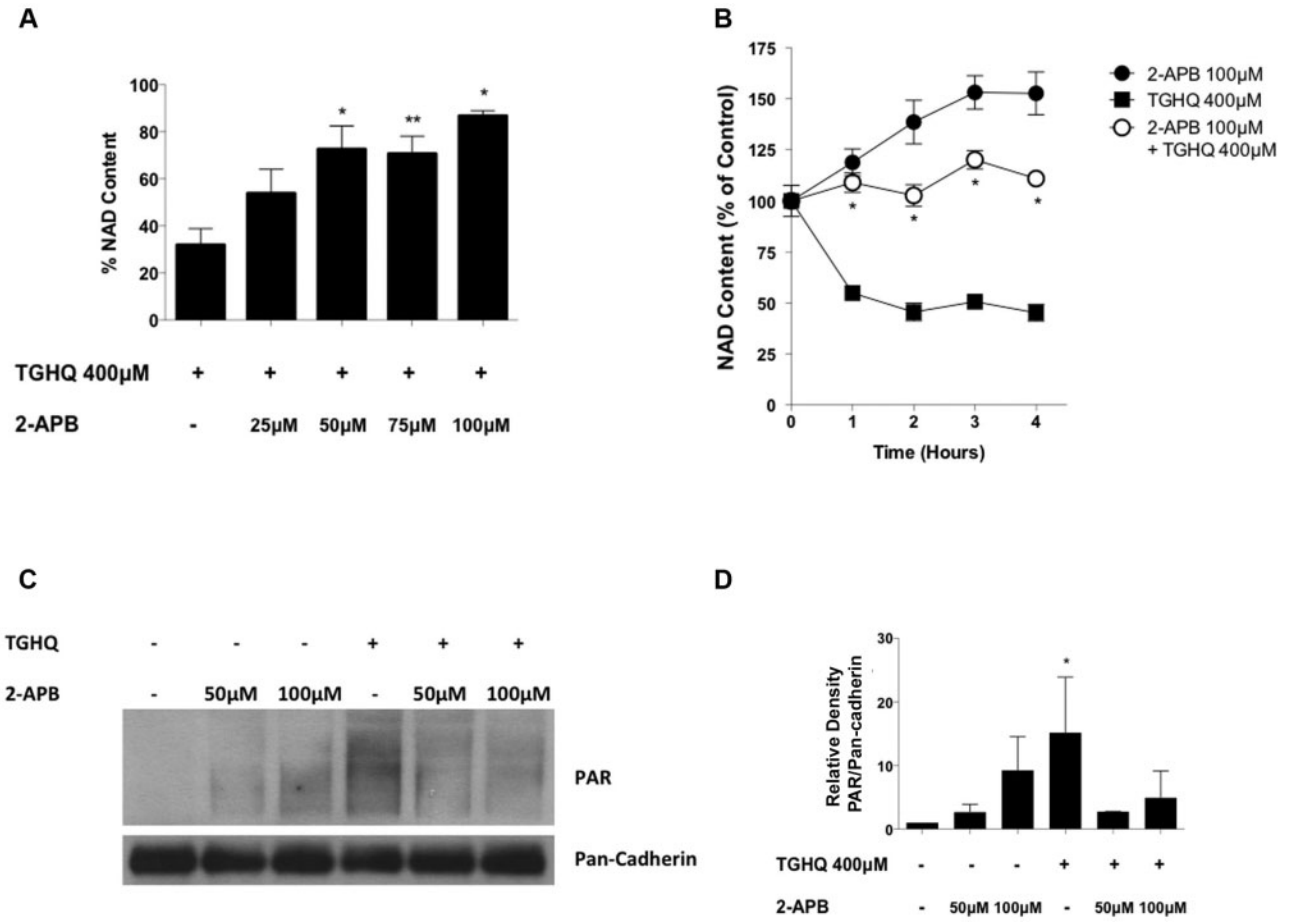

Figure 3. SOC entry is coupled to PARP-1 activation. (A) HK-2 cells were pretreated 30 min with 2-APB at various concentrations (25–100 μM) then co-treated with TGHQ 400 μM. Total NAD^+ was measured using the enzymatic cycling assay 2 h after initial TGHQ treatment. Data are mean ± SE; $n \geq 3$. (B) HK-2 cells were pre-treated 30 min with 2-APB 100 μM then co-treated with TGHQ 400 μM at various time points. Total NAD^+ was measured using the enzymatic cycling assay. Data are mean ± SE; $n \geq 3$. Data are mean ± SE; $n \geq 3$. *$P < .05$, **$P < .01$ when compared with TGHQ by one-way ANOVA followed by a post-hoc Tukey's test. (C) HK-2 cells were treated with 400 μM TGHQ for 30 min in the presence and absence of 2-APB (50 and 100 μM). Cells were collected using a PAR lysis buffer and analyzed by Western blot using an anti-PAR antibody. (D) Densitometric and statistical analysis from three independent biological experiments. Data are mean ± SE; $n = 3$. *$P < .05$ when compared with control by one-way ANOVA followed by a post-hoc Tukey's test.

presence of TGHQ (Figs. 3C and 3D), confirming the coupling of SOCs and PARP.

SOC Activation Occurs Downstream of ROS Generation

ROS were measured using H_2DCFDA to verify 2-APB did not inhibit TGHQ-induced cell death upstream of SOC inhibition. TGHQ induced a 2-fold increase in ROS within 1 h, and N-acetylcysteine (NAC) was able to completely abrogate ROS in the presence of the toxicant (Figure 4). In addition, pretreatment with 2-APB failed to prevent ROS production, confirming that the inhibitory effects of 2-APB on SOCs occur independent of any effects on ROS production.

To further assess whether Ca^{2+} entry through SOCs is coupled to PARP-1-mediated cell death, we determined whether inhibitors of SOCs and PARP could create synergistic or additive cytoprotection in the presence of TGHQ. While each individual inhibitor produced partial protection from TGHQ toxicity, pretreatment and co-treatment with low concentrations of both 2-APB (75 μM) and DPQ (20 μM), a PARP-1 inhibitor, demonstrated no additive or synergistic cytoprotection (Figure 5), consistent with the view that SOCs and PARP-1 are coupled, rather than independently engaged during TGHQ-induced cell death.

Coupling of PARP-1 and Calcium Is Independent of PAR Breakdown by PARG

While PARP-1 ribosylates DNA repair proteins to assist in their recruitment to the site of injury, PARG essentially disassembles these polymers, with the concomitant generation of ADPR, a signaling molecule capable of activating Ca^{2+} channels, such as the TRPM2 cation channel (Naziroglu, 2007). Interestingly however, complete knockdown of PARG (Figure 6C) had no cytoprotection of TGHQ-induced cell death (Figs. 6A and 6B), suggesting that ADPR is not responsible for inducing elevations in iCa^{2+}. However, Western blot analysis confirmed that PARG knockdown increased protein PARylation in the absence of TGHQ (Figs. 6D and 6E), indicating PARG is essential for the breakdown of PAR.

Cystosolic PAR Polymers Post-TGHQ Treatment

Immunofluorescence microscopy revealed that shortly after treatment of cells with TGHQ, PAR polymers were, as anticipated, predominantly located in the nucleus (Figure 7). Intriguingly, at later time points, PARylation was evident in the cytosol, and by 45 min was evenly distributed throughout the cell. Indeed, 60–75 min post-treatment, PARylation was located mainly in the cytosol. The presence of PAR polymers in the cytosol is supportive of a potential role in signaling to ligand-gated Ca^{2+} channels to facilitate Ca^{2+} entry.

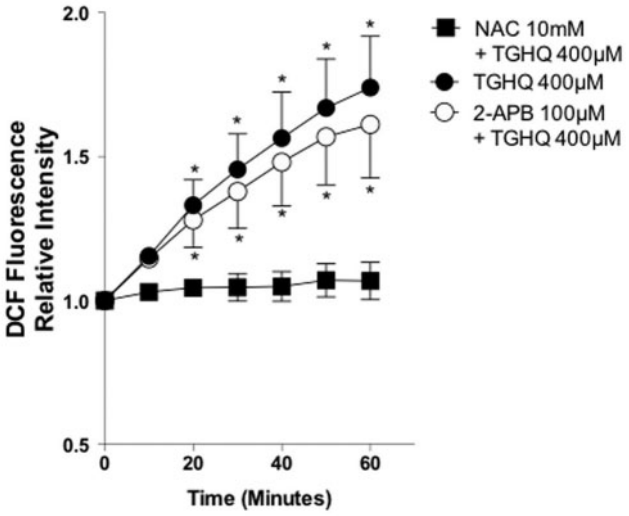

Figure 4. SOC activation occurs downstream of ROS generation. HK-2 cells were incubated with H_2DCFDA (10 μM) for 30 min. Cells were then pre-treated for 30 min with 2-APB (100 μM) or with NAC (10 mM) in the presence of TGHQ 400 μM for 1 h. Fluorescence intensity was measured every 10 min. Data are mean ± SE ($n \geq 3$). *$P < .05$ relative to control fluorescence at time 0 by one-way ANOVA followed by a post-hoc Tukey's test.

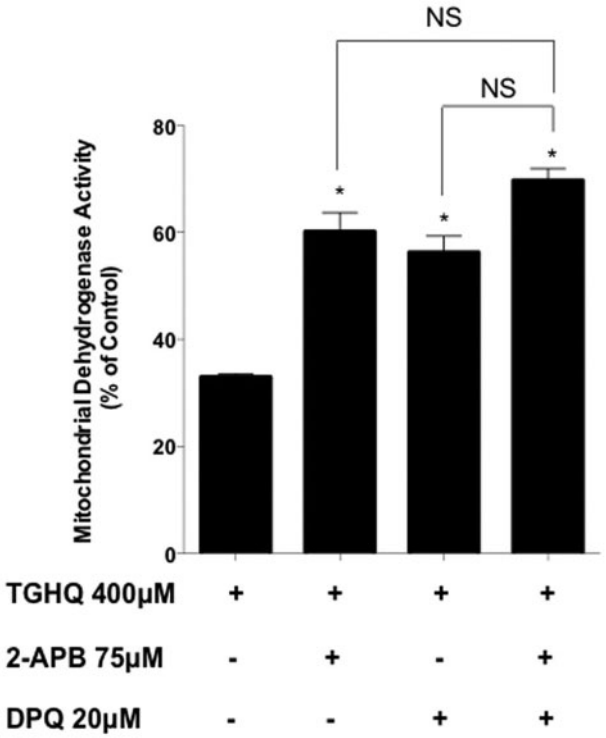

Figure 5. PARP-1 and SOC activation are contiguous and not parallel pathways. HK-2 cells were pre-treated 30 min and co-treated with 2-APB (75 μM) and/or DPQ (20 μM) in the presence of TGHQ 400 μM for 2 h. Cell viability was determined using the MTS based assay. Data are mean ± SE; $n \geq 3$. *$P < .05$ when compared with TGHQ by one-way ANOVA followed by a post-hoc Tukey's test.

DISCUSSION

Human renal proximal tubule epithelial cells (HK-2) exposed to a ROS generating agent (TGHQ) experience an increase in iCa^{2+} concentrations in a PARP-1-dependent manner (Zhang *et al.*, 2014). Thus, PARP-1 hyperactivation and reciprocal elevations in iCa^{2+} are coupled during ROS-induced cell death (Zhang *et al.*, 2014). In this study, we demonstrate that ROS-dependent increases in iCa^{2+} appear to be primarily due to the activation of SOCs (Figure 2). Consistent with this view, inhibition of SOCs prevents increases in iCa^{2+} and restores ROS-mediated depletions in NAD^+ and increases in PARylation caused by the hyperactivation of PARP-1 (Figure 3). Interestingly, previous reports have found that ROS generation can activate SOC entry (Ehring *et al.*, 2000; Hu *et al.*, 2000; Madesh *et al.*, 2005; Nunes and Demaurex, 2014). The two components of SOCs, STIM (STIM1,2), and Orai (Orai 1,2,3) CRAC channels, can be activated through increases in ROS (Bogeski *et al.*, 2010; Gandhirajan *et al.*, 2013; Hawkins *et al.*, 2010). Moreover, cytosolic Ca^{2+} increases are required for PARP-1 activation, and can contribute to PARP-1 hyperactivation (Homburg *et al.*, 2000; Kun *et al.*, 2004; Virag *et al.*, 1999). Thus, TGHQ-induced ROS generation may contribute to SOC activation and lead to further PARP-1 activation.

Conversely, TGHQ-mediated PARP-1 hyperactivation causes an increase in protein PARylation (Figure 3C). PARylation plays a diverse role in many cellular and molecular processes (Kim *et al.*, 2005). Recent proteome-wide identification of PARylated proteins revealed PARylation of Ca^{2+}-related proteins, including the SERCA pump (Gagne *et al.*, 2008; Pic *et al.*, 2011). Therefore, we speculate that SOCs may also be activated through increased PARylation of Ca^{2+}-related proteins that leads to increases in iCa^{2+} and subsequently, exacerbates PARP-1 hyperactivation. SOCs are ubiquitously expressed channels comprised of 2 major components, STIM1/2 and Orai1,2,3 (Lewis, 2011). Orai proteins, also known as CRAC channels, are located on the plasma membrane, while STIM1/2 are located on the ER (Prakriya and Lewis, 2015). When intracellular ER Ca^{2+} stores are depleted, STIM1/2 translocate to the plasma membrane to open CRAC channels, thus allowing for Ca^{2+} entry (Lewis, 2011; Prakriya and Lewis, 2015). Since SOCs are expressed in HK-2 cells and primary human proximal tubular cells (Garcia-Vaz *et al.*, 2014; Mai *et al.*, 2016), it may be possible that PARylation of the SERCA pump, located on the ER, can indirectly induce SOC activation, and thus iCa^{2+} entry to the ER and cytosol that leads to cell death.

Breakdown of PAR to ADPR is catalyzed by PARG (Davidovic *et al.*, 2001) and the coupling of PARP-1 and Ca^{2+} through PARG breakdown of PAR to ADPR is well established; indeed, the import of extracellular Ca^{2+} through the melastatin-like transient receptor potential 2 channels (TRPM2), a cation permeable channel activated by ADPR, contributes to store-operated Ca^{2+} entry. Activation of TRPM2 accounts for the Ca^{2+} influx into the cytosol, and ultimately to cell death in mouse embryonic fibroblasts and macrophages (Blenn *et al.*, 2011; Zou *et al.*, 2013). Moreover, PARG silencing in these cells can protect against ROS-induced cell death (Blenn *et al.*, 2006; Zou *et al.*, 2013), implying that the disassembly of PAR polymers is necessary for downstream signaling coupled to PARP-mediated cell death. Indeed, PAR is viewed as playing an active role in cell death in complex ways that seem to be cell- or tissue-specific (Luo and Kraus, 2012). For example, PAR polymers are directly toxic to neurons during *N*-methyl-*N*-nitro-*N*-nitrosoguanidine-induced cell death, and PARG mediated PAR breakdown can protect against cell death (Andrabi *et al.*, 2006). We demonstrated the ability of PAR to translocate from the nucleus to the cytosol of HK-2 cells (Figure 7), and the export of PAR from the nucleus triggers the release of the AIF from mitochondria, ultimately mediating a caspase-independent cell death (parthantos) (Virag *et al.*, 2013). Conversely, in HL-60 cells, human promyelocytic leukemia cells, PAR proteins are detected following TGHQ treatment, and AIF is released from mitochondria and migrates to

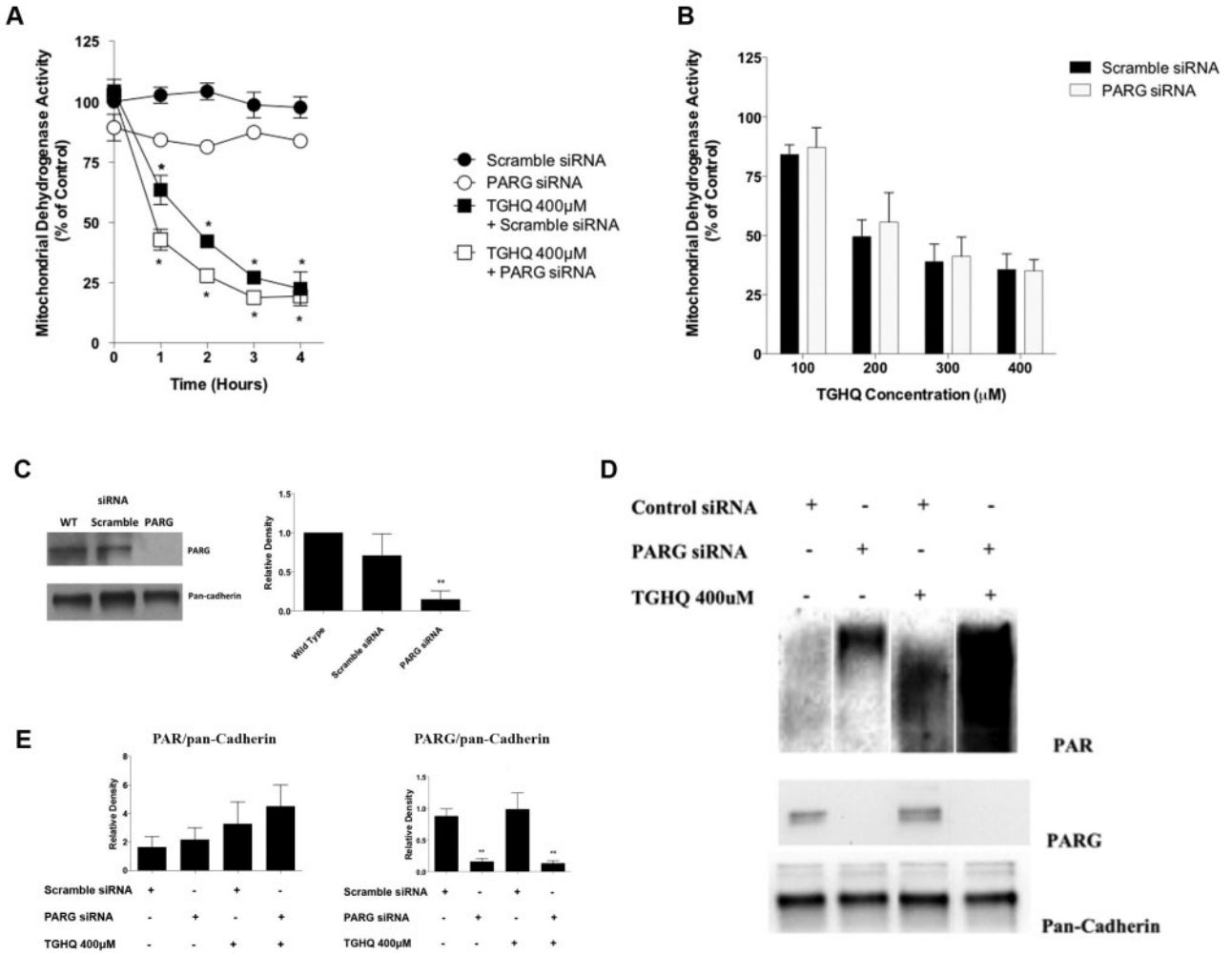

Figure 6. PARP-1-mediated cell death is independent of PAR processing by PARG. (A) Cells were transfected using 25 nM non-targeting scramble siRNA or PARG siRNA and incubated for 72 h. HK-2 cells were treated with TGHQ 400 μM at various time points (1–4 h). Cell viability was determined using the MTS-based assay. Data are mean ± SE ($n \geq 3$) relative to their respective siRNA controls. *$P < .05$ when compared with control by one-way ANOVA followed by a post-hoc Tukey's test. (B) Cells were transfected using 25 nM non-targeting scramble siRNA or PARG siRNA and incubated for 72 h. HK-2 cells were treated with TGHQ (100–400 μM) in the presence of scramble siRNA or PARG siRNA for 2 h. Cell viability was determined using the MTS-based assay, measuring mitochondrial dehydrogenase activity. Data are mean ± SE ($n \geq 3$) relative to their respective siRNA controls. (C) Western blot analysis was performed using anti-PARG, with pan-cadherin as a loading control. **$P < .01$ when compared with WT by one-way ANOVA followed by a post-hoc Tukey's test. (D) HK-2 cells were treated with TGHQ 400 μM for 30 min in the presence of Scramble siRNA or PARG siRNA. Cells were collected using PAR lysis buffer analyzed by Western blot using anti-PAR antibody, anti-PARG, and pan-cadherin as a loading control. (E) Densitometric and statistical analysis of siRNA knockdown confirmation from three independent experiments. Data are mean ± SE; $n \geq 3$. **$P < .01$ when compared with scramble siRNA by one-way ANOVA followed by a post-hoc Tukey's test.

the nucleus (Zhang *et al.*, 2012). However, TGHQ-induced apoptosis of HL-60 cells is caspase dependent (Zhang *et al.*, 2012). Clearly, the mechanisms by which nuclear protein PARylation couples to downstream cytosolic signaling and ultimately cell death is complex and context dependent.

PARG silencing did not restore mitochondrial dehydrogenase activity (Figs. 6A–C). PARG, nevertheless, is clearly active in HK-2 cells and can break down PAR polymers in both the presence and absence of TGHQ, as PARylation increased during PARG silencing (Figs. 6D and 6E). Thus, our data indicate a novel PARG-independent cell death pathway that may require PARylation of proteins rather than the breakdown of PARylation to ADPR. These data are consistent with previous findings in HK-2 cells where ROS-induced cell death was independent of mitochondrial AIF release (Zhang *et al.*, 2014), a PAR-dependent process.

Our previous report on HK-2 cells demonstrated ROS increases occurred as early as 5–10 min, PAR polymer formation was seen between 15 and 30 min, and iCa^{2+} increases occurred after 35 min. Consistent with these results, this study demonstrated PAR formation in the nucleus at 15 min post-TGHQ application (Figure 7), suggesting PARP-1 activation due to ROS increases. Moreover, PAR polymer migration to the cytosol occurs between 30 and 45 min (Figure 7), consistent with subsequent increases in iCa^{2+} observed between 35 and 45 min. Thus, in our current model, we speculate that TGHQ produces robust ROS increases and DNA damage, which lead to activation of PARP-1 and PAR polymer formation, and subsequent increases in iCa^{2+} through SOCs activation that lead to non-apoptotic cell death (Figure 8).

In summary, in the HK-2 cell model of ROS-induced non-apoptotic cell death, SOCs are coupled to PARP-1 hyperactivation (Figure 3) and the subsequent excessive protein PARylation appears to activate a PARG-independent pathway to cell death that may facilitate extracellular Ca^{2+} entry through SOCs.

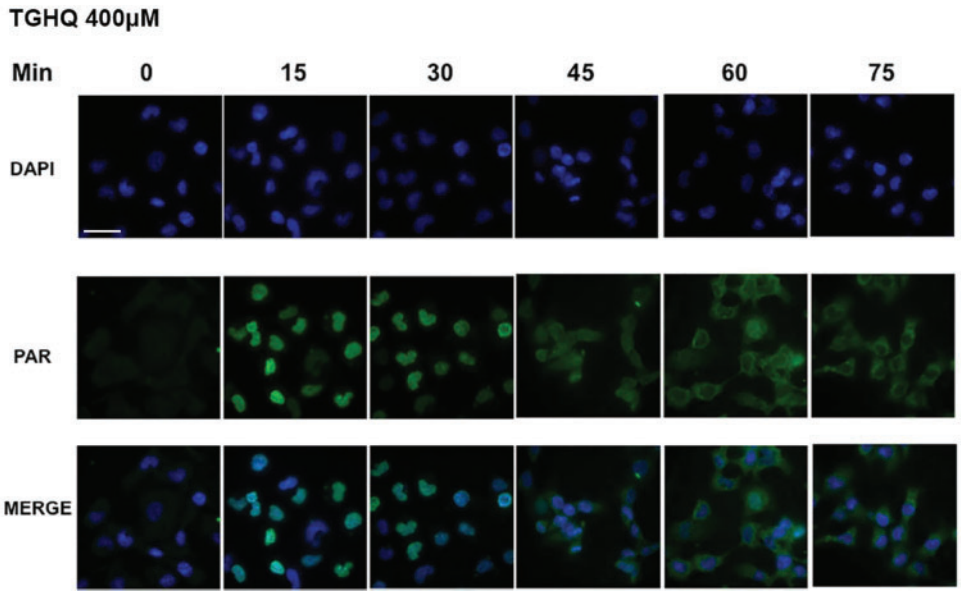

Figure 7. Identification of cytosolic PAR following TGHQ treatment. HK-2 cells were treated with 400 μM TGHQ for various time periods (0–75 min). Cells were fixed in a 1:1 MeOH:acetone solution and probed with anti-PAR antibody, then incubated with Alexa Fluor 488 secondary antibody and DAPI stain. Cells were imaged using ×40 magnification on a deconvolution microscope and images were collected using DeltaVision softWoRx. Images were analyzed using the NIH provided software ImageJ. Scale bar 100 μm.

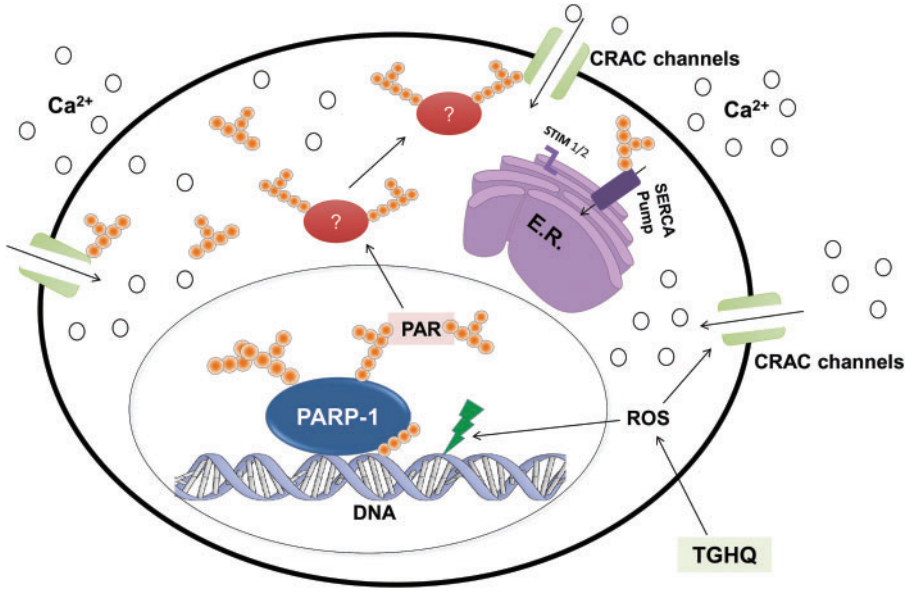

Figure 8. Proposed model of TGHQ-induced PARP-1-mediated non-apoptotic cell death in HK-2 cells. TGHQ, a potent nephrotoxic and carcinogenic metabolite of HQ, induces the robust generation of ROS, which leads to DNA damage and the hyperactivation of PARP-1. Activated PARP-1 subsequently depletes NAD^+ to create PAR polymers, which translocate from the nucleus to the cytosol, thus PARylating proteins that may lead to activation of SOCs (CRAC channels). Activation of CRAC channels may also occur directly through ROS or direct PARylation. The subsequent iCa^{2+} increases may lead to non-apoptotic cell death. Green lightning represents ROS-induced DNA damage, pink spheres represent Ca^{2+}, PAR is represented by orange spheres in chains, and red ovals represent possible PARylated proteins involved in TGHQ-mediated cell death.

Protein PARylation *per se* could represent a cell death signal, activating downstream signaling pathways that contribute to increases in iCa^{2+}, further exacerbating cell death. Our studies reveal a novel PARP-1-dependent, PARG-independent cell death pathway. The PARG-independent nature of cell death is consistent with findings that indicate a PARP-dependent, AIF-independent pathway to cell death (Zhang *et al.*, 2014). We speculate that PARylation of cytosolic proteins causes downstream signaling, activating store-operated Ca^{2+} entry, ultimately increasing iCa^{2+} concentrations, and leading to PARP-1-dependent cell death. To further elucidate the role of PARylated proteins in cell death, current studies are focused on the identification of PAR-modified proteins following TGHQ exposure.

ACKNOWLEDGMENTS

We would like to thank Dr David Elliot for assistance with, and use of, the deconvolution microscope for the calcium

imaging studies, and Dr Doug Cromey, from the Cell Imaging Core of the South West Environmental Health Sciences Center, for his assistance with immunofluorescence and data analysis.

FUNDING

This study was supported in part by an award to SSL from the National Institute of Environmental Health Sciences (P30ES006694), and to F.Z. from the National Natural Science Foundation of China (21507093); Natural Science Foundation of Liaoning Province (2015020737); Fund for long-term training of young teachers in Shenyang Pharmaceutical University (ZCJJ2014402); and the General project of Education Department of Liaoning Province (L2015529).

REFERENCES

Andrabi, S. A., Kim, N. S., Yu, S. W., Wang, H., Koh, D. W., Sasaki, M., Klaus, J. A., Otsuka, T., Zhang, Z., Koehler, R. C., *et al.* (2006). Poly(ADP-ribose) (PAR) polymer is a death signal. *Proc. Natl Acad. Sci. U. S. A.* **103**, 18308–18313.

Bentle, M. S., Reinicke, K. E., Bey, E. A., Spitz, D. R., and Boothman, D. A. (2006). Calcium-dependent modulation of poly(ADP-ribose) polymerase-1 alters cellular metabolism and DNA repair. *J. Biol. Chem.* **281**, 33684–33696.

Blenn, C., Althaus, F. R., and Malanga, M. (2006). Poly(ADP-ribose) glycohydrolase silencing protects against H2O2-induced cell death. *Biochem. J.* **396**, 419–429.

Blenn, C., Wyrsch, P., Bader, J., Bollhalder, M., and Althaus, F. R. (2011). Poly(ADP-ribose)glycohydrolase is an upstream regulator of Ca2+ fluxes in oxidative cell death. *Cell Mol. Life Sci.* **68**, 1455–1466.

Bogeski, I., Kummerow, C., Al-Ansary, D., Schwarz, E. C., Koehler, R., Kozai, D., Takahashi, N., Peinelt, C., Griesemer, D., Bozem, M., *et al.* (2010). Differential redox regulation of ORAI ion channels: a mechanism to tune cellular calcium signaling. *Sci. Signal.* **3**, ra24.

D'Amours, D., Desnoyers, S., D'Silva, I., and Poirier, G. G. (1999). Poly(ADP-ribosyl)ation reactions in the regulation of nuclear functions. *Biochem. J.* **342**, 249–268.

Davidovic, L., Vodenicharov, M., Affar, E. B., and Poirier, G. G. (2001). Importance of poly(ADP-ribose) glycohydrolase in the control of poly(ADP-ribose) metabolism. *Exp. Cell Res.* **268**, 7–13.

DeHaven, W. I., Smyth, J. T., Boyles, R. R., Bird, G. S., and Putney, J. W. Jr. (2008). Complex actions of 2-aminoethyldiphenyl borate on store-operated calcium entry. *J. Biol. Chem.* **283**, 19265–19273.

Ehring, G. R., Kerschbaum, H. H., Fanger, C. M., Eder, C., Rauer, H., and Cahalan, M. D. (2000). Vanadate induces calcium signaling, Ca2+ release-activated Ca2+ channel activation, and gene expression in T lymphocytes and RBL-2H3 mast cells via thiol oxidation. *J. Immunol.* **164**, 679–687.

Gagne, J. P., Isabelle, M., Lo, K. S., Bourassa, S., Hendzel, M. J., Dawson, V. L., Dawson, T. M., and Poirier, G. G. (2008). Proteome-wide identification of poly(ADP-ribose) binding proteins and poly(ADP-ribose)-associated protein complexes. *Nucleic Acids Res.* **36**, 6959–6976.

Gagne, J. P., Shah, R. G., and Poirier, G. G. (2001). Analysis of ADP-ribose polymer sizes in intact cells. *Mol. Cell. Biochem.* **224**, 183–185.

Gandhirajan, R. K., Meng, S., Chandramoorthy, H. C., Mallilankaraman, K., Mancarella, S., Gao, H., Razmpour, R., Yang, X. F., Houser, S. R., Chen, J., *et al.* (2013). Blockade of NOX2 and STIM1 signaling limits lipopolysaccharide-induced vascular inflammation. *J. Clin. Invest.* **123**, 887–902.

Garcia-Vaz, E., Chen, G., Bhandari, S., Daskoulidou, N., Zeng, B., Jiang, H., Gomez, M. F., Atkin, S. L., and Xu, S. (2014). ORAI store-operated calcium channels are associated with proximal renal tubule dysfunction in diabetic nephropathy. *FASEB J* **28** 689.13.

Hawkins, B. J., Irrinki, K. M., Mallilankaraman, K., Lien, Y. C., Wang, Y., Bhanumathy, C. D., Subbiah, R., Ritchie, M. F., Soboloff, J., Baba, Y., *et al.* (2010). S-glutathionylation activates STIM1 and alters mitochondrial homeostasis. *J. Cell Biol.* **190**, 391–405.

Homburg, S., Visochek, L., Moran, N., Dantzer, F., Priel, E., Asculai, E., Schwartz, D., Rotter, V., Dekel, N., and Cohen-Armon, M. (2000). A fast signal-induced activation of Poly(ADP-ribose) polymerase. A novel downstream target of Phospholipase c. *J. Cell Biol.* **150**, 293–307.

Hu, Q., Zheng, G., Zweier, J. L., Deshpande, S., Irani, K., and Ziegelstein, R. C. (2000). NADPH oxidase activation increases the sensitivity of intracellular Ca2+ stores to inositol 1,4,5-trisphosphate in human endothelial cells. *J. Biol. Chem.* **275**, 15749–15757.

Jacobson, E. L., and Jacobson, M. K. (1997). Tissue NAD as a biochemical measure of niacin status in humans. *Methods Enzymol.* **280**, 221–230.

Jagtap, P., and Szabo, C. (2005). Poly(ADP-ribose) polymerase and the therapeutic effects of its inhibitors. *Nat. Rev. Drug Discov.* **4**, 421–440.

Kim, M. Y., Zhang, T., and Kraus, W. L. (2005). Poly(ADP-ribosyl)ation by PARP-1: 'PAR-laying' NAD+ into a nuclear signal. *Genes Dev.* **19**, 1951–1967.

Kraus, W. L. (2008). Transcriptional control by PARP-1: chromatin modulation, enhancer-binding, coregulation, and insulation. *Curr. Opin. Cell Biol.* **20**, 294–302.

Krishnakumar, R., and Kraus, W. L. (2010). The PARP side of the nucleus: molecular actions, physiological outcomes, and clinical targets. *Mol. Cell* **39**, 8–24.

Kun, E., Kirsten, E., Mendeleyev, J., and Ordahl, C. P. (2004). Regulation of the enzymatic catalysis of poly(ADP-ribose) polymerase by dsDNA, polyamines, Mg2+, Ca2+, histones H1 and H3, and ATP. *Biochemistry* **43**, 210–216.

Lau, S. S., McMenamin, M. G., and Monks, T. J. (1988). Differential uptake of isomeric 2-bromohydroquinone-glutathione conjugates into kidney slices. *Biochem. Biophys. Res. Commun.* **152**, 223–230.

Lau, S. S., Monks, T. J., Everitt, J. I., Kleymenova, E., and Walker, C. L. (2001). Carcinogenicity of a nephrotoxic metabolite of the "nongenotoxic" carcinogen hydroquinone. *Chem. Res. Toxicol.* **14**, 25–33.

Lewis, R. S. (2011). Store-operated calcium channels: new perspectives on mechanism and function. *Cold Spring Harb. Perspect. Biol.* **3**, 3970.

Luo, X., and Kraus, W. L. (2012). On PAR with PARP: cellular stress signaling through poly(ADP-ribose) and PARP-1. *Genes Dev.* **26**, 417–432.

Madesh, M., Hawkins, B. J., Milovanova, T., Bhanumathy, C. D., Joseph, S. K., Ramachandrarao, S. P., Sharma, K., Kurosaki, T., and Fisher, A. B. (2005). Selective role for superoxide in InsP3 receptor-mediated mitochondrial dysfunction and endothelial apoptosis. *J. Cell Biol.* **170**, 1079–1090.

Mai, X., Shang, J., Liang, S., Yu, B., Yuan, J., Lin, Y., Luo, R., Zhang, F., Liu, Y., Lv, X., *et al.* (2016). Blockade of Orai1 store-operated calcium entry protects against renal fibrosis. *J. Am. Soc. Nephrol.* **27**, 3063–3078.

Munoz-Gamez, J. A., Rodriguez-Vargas, J. M., Quiles-Perez, R., Aguilar-Quesada, R., Martin-Oliva, D., de Murcia, G., Menissier de Murcia, J., Almendros, A., Ruiz de Almodovar, M., and Oliver, F. J. (2009). PARP-1 is involved in autophagy induced by DNA damage. *Autophagy* **5**, 61–74.

Naziroglu, M. (2007). New molecular mechanisms on the activation of TRPM2 channels by oxidative stress and ADP-ribose. *Neurochem. Res.* **32**, 1990–2001.

Nunes, P., and Demaurex, N. (2014). Redox regulation of store-operated Ca2+ entry. *Antioxid. Redox Signal.* **21**, 915–932.

Pic, E., Gagne, J. P., and Poirier, G. G. (2011). Mass spectrometry-based functional proteomics of poly(ADP-ribose) polymerase-1. *Expert Rev. Proteomics* **8**, 759–774.

Pieper, A. A., Verma, A., Zhang, J., and Snyder, S. H. (1999). Poly (ADP-ribose) polymerase, nitric oxide and cell death. *Trends Pharmacol. Sci.* **20**, 171–181.

Prakriya, M., and Lewis, R. S. (2015). Store-operated calcium channels. *Physiol. Rev.* **95**, 1383–1436.

Rodriguez-Vargas, J. M., Ruiz-Magana, M. J., Ruiz-Ruiz, C., Majuelos-Melguizo, J., Peralta-Leal, A., Rodriguez, M. I., Munoz-Gamez, J. A., de Almodovar, M. R., Siles, E., Rivas, A. L., *et al.* (2012). ROS-induced DNA damage and PARP-1 are required for optimal induction of starvation-induced autophagy. *Cell Res.* **22**, 1181–1198.

Virag, L., Robaszkiewicz, A., Rodriguez-Vargas, J. M., and Oliver, F. J. (2013). Poly(ADP-ribose) signaling in cell death. *Mol. Aspects Med.* **34**, 1153–1167.

Virag, L., Salzman, A. L., and Szabo, C. (1998). Poly(ADP-ribose) synthetase activation mediates mitochondrial injury during oxidant-induced cell death. *J. Immunol.* **161**, 3753–3759.

Virag, L., Scott, G. S., Antal-Szalmas, P., O'Connor, M., Ohshima, H., and Szabo, C. (1999). Requirement of intracellular calcium mobilization for peroxynitrite-induced poly(ADP-ribose) synthetase activation and cytotoxicity. *Mol. Pharmacol.* **56**, 824–833.

Zhang, F., Lau, S. S., and Monks, T. J. (2012). A dual role for poly(ADP-ribose) polymerase-1 during caspase-dependent apoptosis. *Toxicol. Sci.* **128**, 103–114.

Zhang, F., Xie, R., Munoz, F. M., Lau, S. S., and Monks, T. J. (2014). PARP-1 hyperactivation and reciprocal elevations in intracellular Ca2+ during ROS-induced nonapoptotic cell death. *Toxicol. Sci.* **140**, 118–134.

Zou, J., Ainscough, J. F., Yang, W., Sedo, A., Yu, S. P., Mei, Z. Z., Sivaprasadarao, A., Beech, D. J., and Jiang, L. H. (2013). A differential role of macrophage TRPM2 channels in Ca(2)(+) signaling and cell death in early responses to H(2)O(2). *Am. J. Physiol. Cell. Physiol.* **305**, C61–C69.